2023

Semi-Robotic Knee Arthroscopy System with Braking Mechanism

Thai Hua
University of Central Florida

SEMI-ROBOTIC KNEE ARTHROSCOPY SYSTEM WITH BRAKING MECHANISM

by

THAI T. HUA

A thesis submitted in partial fulfillment of the requirements

for the Honors in the Major Program in Mechanical Engineering

in the College of Engineering and Computer Science

and in the Burnett Honors College

at the University of Central Florida

Orlando, Florida

Spring Term, 2023

Thesis Chair: Yuanli Bai, Ph.D.

Thesis Committee Members: Hwan Choi, Ph.D., Joon-Hyuk Park, Ph.D.

Abstract

To alleviate the poor ergonomics which surgeons suffer during knee arthroscopy, a semi-robotic device with braking mechanism is created for intraoperative assistance. A slitted ball joint assembly is developed to transmit the clamping force to the arthroscope inside. Ball deformation and stress at various angles to the vertical and clamping forces is recorded through Abaqus Finite Element Analysis (FEA). Contact forces between the scope and inner surfaces of the ball is also computed in FEA at different clamping forces. The von Mises stress occurring in the ball joint is under the yield stress limit for polyethylene, and there is noticeable force preventing the scope from sliding along the ball through-hole under clamping. A prototype of this device is constructed for proof-of-concept.

Acknowledgements

I thank Dr. Sang-Eun Song for the research opportunity and the extensive support throughout the first phase of my thesis, giving me the leverage I needed to kickstart my research in the best way.

I thank Dr. Yuanli Bai for assisting me through the second phase of my thesis, lending me much of his expertise which helped me learn the things I needed to complete my research up to present.

To my committee members, Dr. Joon-Hyuk Park and Dr. Hwan Choi, for their valuable time and feedback.

To my parents and friends who have given me plenty of support through the most stressful times, I love you all.

Table of Contents

List of Tables

List of Figures

1. Introduction

1.1 Overall background

In 1958, Dr. Masaki Watanabe developed the 21st scope, the world's first successful arthroscope, deriving from Dr. Kenji Takagi's work on detecting tuberculosis arthritis using knee endoscopy [4]. Nowadays, knee arthroscopy (KA) is a well-established minimally invasive procedure used to diagnose and treat patients' complications in the knee joint, such as osteoarthritis and meniscus tears [5]. Its advantages consist of reduced trauma and recovery time, and fewer surgery-associated complications [6, 7]. The general procedure entails providing anesthesia, then making small skin incisions called "portals", through which the surgeon inserts a trocar, through which tools specific to the operation are inserted. The surgeon then views the inside of the knee on a screen, which shows the images that a camera lens on the end of the arthroscope captures.

Moreover. researchers have expressed interest in automating surgical procedures. Total knee arthroplasty is an open surgical procedure that uses robots to improve clinical outcomes, such as the Stryker/MAKO system [8]. Laparoscopic surgery is also supported by the da Vinci robot by Intuitive Surgical Inc. [9] Vitiello et al. [7] explains the technological advancements – such as better imaging and sensing - that gave way to better surgical platforms used for a wide variety of procedures. In current practice, the automation procedure exhibits a master-slave relationship between the surgeon and the robot [10]. Not only are surgical robots safe, but they may also be more effective than conventional techniques [11].

Despite various advancements in the surgical robotics field, there is yet to be a fully autonomous system for specifically knee arthroscopy [12]. However, there exists commercial

systems used to provide computer navigation during KA, such as the AESCULAP® OrthoPilot and the Northern Digital® Polaris Spectra. In anterior cruciate ligament reconstruction (ACLR), the OrthoPilot can provide precise tibial and femoral tunnel placements [13, 14]. Planning of tunnel placement can also be assisted by a fluoroscopic overlay [15, 16], magnetic resonance imaging (MRI) [15, 16], or other surface-based registration methods. Such computer navigation can prevent posterior wall blowouts [17, 18] and prevent complications related to poor tunnel positioning, hence its large-scale feasibility in supporting ACLR.[19] Computer navigation, though only semi-autonomous, offers great help to surgeons intraoperatively, allowing for better clinical results and less strain on the surgeons.

Researchers have also developed simulator devices to train interning residents. Their features may include visual and haptic feedback, instrumented probe and tools, 3D reconstruction of knee anatomy, virtual tracking of tools, and real-time anatomy mechanics with collision detection, tissue deformation and cutting [20-23]. Alongside KA simulation, some systems may have learning modules where trainees can test their anatomy and procedural knowledge [24], while others can give performance feedback of simulated tasks. Just as expected in the actual procedure, senior residents perform better than junior residents in simulated KA [25], even under distraction [26]. However, simulation platforms have shown to be effectual in facilitating learning for intern residents, and may result in greater performance in the actual procedure [20, 27]. Though these simulators can be viewed as virtual reality platforms, they can combine with computer navigation methods to provide real time augmented virtuality, which allows for better visualization and planning of the procedure. Thus, they represent a significant part of the current technology in KA.

For truly autonomous KA, necessary components include sensing and localization, path planning, and computer vision. Though these features are present in some KA platforms for research, their clinical adaptability has not been determined. Future research should aim to involve these technologies intraoperatively and evaluate their effectiveness when used by surgeons.

1.2 Conventional Procedure

In minimally invasive surgery (MIS), the surgeon makes small incisions near the surgical field, through which surgical tools are inserted. The surgeon sees the intra-articular structures through a camera lens attached to the end of an arthroscope, as images recorded are projected onto a screen for viewing. The general procedure for KA entails providing anesthesia, then making small skin incisions called “portals”, through which the surgeon inserts a cannula, through which tools specific to the operation are inserted. The location of these portals varies across different types of knee arthroscopic procedures [5, 6]. Common portals include the anteromedial portal – made medial to the medial border of the patella tendon – and the anterolateral portal – made approximately 1 cm above the joint line and in line with the lateral border of the patella [5]. The superolateral portal can also be made for irrigation. Some apparatuses are present in every arthroscopic procedure, such as an arthroscope. Different arthroscopes have different fields of view, and each is selected depending on the requirements of the operation [6].

Some common arthroscopic procedures of the knee are meniscus repair and meniscectomy. Per a study in Syracuse, New York, 61 in 100,000 patients with meniscal injury undergo meniscectomy [28]. When a patient has a torn meniscus in the knee joint, resulting in

pain and difficulty walking, the surgeon may decide to either repair or remove some (partial meniscectomy) or all (total meniscectomy) of the meniscus. This procedure requires tools such as a scalpel to make the incision, an arthroscope to see intra-articular structures, and an angled probe to examine the meniscus surface [29]. For repair, the surgeon can suture torn meniscus to healthy meniscus where there is sufficient blood supply to conduct healing. For meniscectomy, a manual cutter and a motorized shaver may be used to remove the torn fibers. As the meniscus serves as a load bearer and stabilizer for the knee joint, one must attempt to preserve as much healthy meniscus as possible [30]. For this reason, meniscal repair, if possible, is preferred to meniscectomy.

Procedures can range in complexity, from simple ones such as diagnosis and probing, to more complex ones like meniscal transplant, ACLR, and mosaicplasty. Conventionally, the surgeon is accompanied by their assistant, the scrub nurse, the scrub scout nurse, and the anesthetist. During the procedure, the surgeon wields a tool in each hand, changes the patient's knee flexion, and alternates between looking at the operating field and the monitor showing arthroscope recording. As KA is a minimally invasive procedure, certain challenges are present, which will be discussed below.

1.3 Robotic Procedure

1.3.1 Sensing, localization, path planning

Sensing and localization are crucial to measuring the position and orientation of a tool, making sure that it does not damage surrounding tissue. Path planning uses the odometry of a tool to produce a path for the tool tip to reach target anatomy while navigating through anatomical obstacles. In conventional arthroscopy, the surgeon can only see the inside of the

knee through the arthroscope camera recording and may change the knee flexion/extension angle to gain better intraarticular access. Therefore, having these technologies during KA can be helpful, even if the device is not fully robotic.

For handheld tools, one can find sensors in arthroscopes with a flexible end-effector to measure the tip position with respect to the centroidal axis, as well as the forces and torques occurring at the tip. An example of a mechanism allowing such a flexible end effector can be seen in Fig. 1. Wishing to accompany similar mechanisms in arthroscopes, Cui et al. [31] developed a sensor to measure reaction forces and moments when the arthroscope is in contact with surrounding tissue, ensuring that the contact does not cause iatrogenic damage (see Fig. 3a). Moreover, Yan Nai et al. [2] incorporates both a force and position sensor in their flexible distal manipulator, whose signals are fed through a data acquisition module and amplified for computer processing – the schematic for this device is found in Fig. 2. Osteochondral grafts can also be realized using a rigid tool – Long et al. [32] use electromagnetic sensors for real time 3D visualization and navigation of the procedure, tracking the harvester tool and endoscope. These devices can provide another source of feedback to the surgeon, but their full potential is better reflected on externally mounted surgical platforms. Applications include visual servoing of cartilage tissue [33] and flexoscope for laser osteotomy [34, 35], shown in Fig. 3b and Fig. 3c. For automation, sensing of reaction forces and torques is important for the safety of the patient, and sensing of joint angles is important to the kinematics and path planning attributes of the system. They form a crucial part of feedback loops for controls.

Moreover, established techniques include Simultaneous Localization and Mapping (SLAM), commonly used to provide tool tracking during the procedure. Marmol et al. [3] apply

SLAM to reliably localize the arthroscope during KA, fusing information acquired from sensors on the arthroscope, an external camera mounted to the robotic arthroscope manipulator, and the odometry of the arm manipulator in an Extended Kalman Filter, all of which are graphically shown in Fig. 4. Similarly, path planning is done by computational methods. Razjigaev et al. [36] develop SnakeRaven, a 3D printed dexterous end-effector to reach target anatomy in the knee joint, navigating through the anatomical obstacles to prevent iatrogenic damage. Path planning is done by optimization of joint angles tested in a 3D voxelization of a scanned knee joint – the dexterity fitness being satisfactory when the end-effector does not coincide with an anatomical voxel. In the same way, Ciszkiewicz and Milewski use surface meshes of the tool and knee to determine an optimized and collision-free path towards a final location [37]. This hybrid optimization method uses Real-Coded Genetic Algorithm to search for a valid path, and Nedler-Mead Method to locally optimize it. Such methods of sensing, localization, and path planning can be useful in semi-autonomous KA to aid the surgeon's decision-making, and in fully autonomous KA for high-level control and closed feedback loops. Nonetheless, with the inputs needed to execute such computations, it is favorable to develop ways in which the platform can autonomously gain that input – using computer vision.

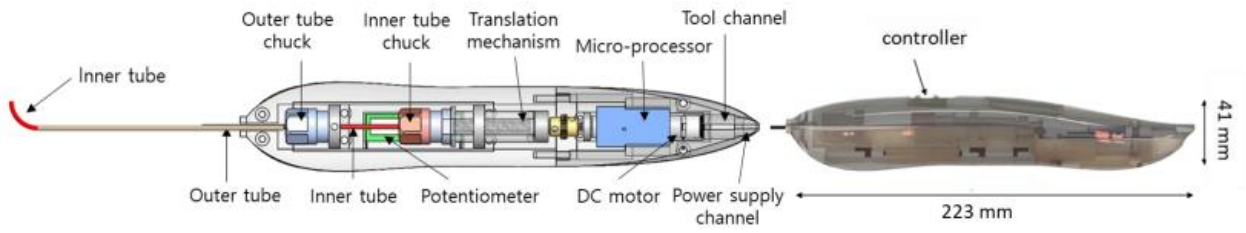

Fig. 1. The device designed in Kim et al. for shoulder arthroscopy [1]. The outer tube is a straight stainless-steel tube, while the inner tube is flexible heat-treated nitinol. The distal tip has 2 DoF: the axial translation by motorized actuation and manual.

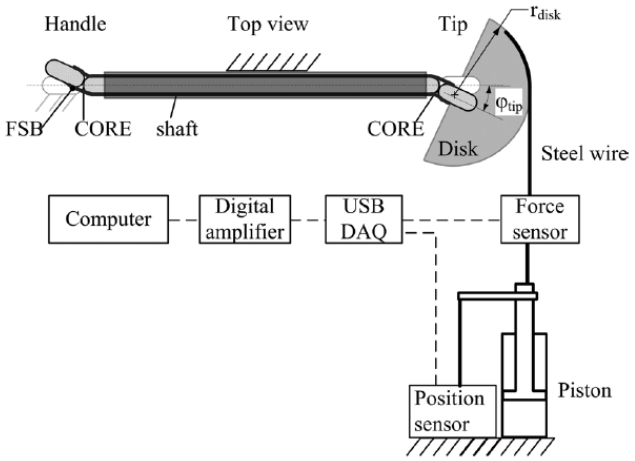

Fig. 2. Schematic of sideways-steerable distal joint for high force transmission, described in Yan Nai et al.[2] Mechanical tests confirmed that the prototype can transmit an axial load of 200 N on the tip with a maximum parasitic deflection of 4.4 degrees.

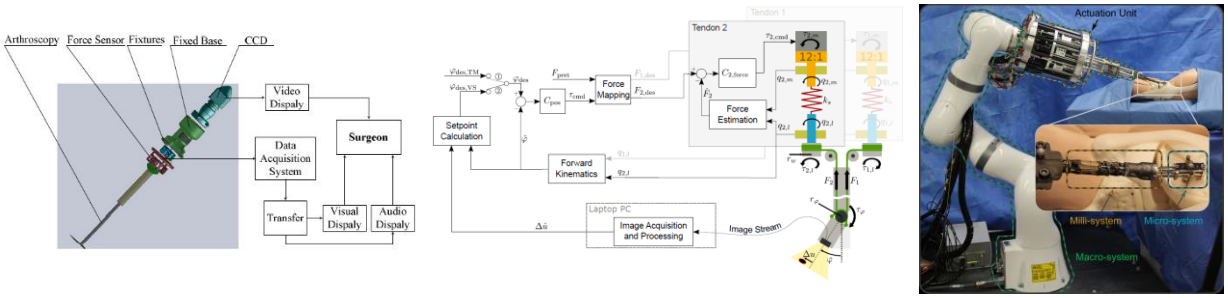

(a) (b) (c)

Fig. 3. (a) Instrument including force sensor developed in Cui et al. [31] Strain gauges measure the deformation of the sensor when reaction forces and moments act upon the instrument. (b) Control scheme of telemanipulation in the visual servoing mechanism in Fasel et al. [33] The distal endoscopic joint has 2 DoF and is driven by two antagonistic tendons. Images collected by the endoscope are acquired with a dedicated board and processed for tracking cartilage. (c) Robotic arm carries all of the macro (serial manipulator), milli (distal flexible endoscope), and micro (laser) components. This system, developed by Eugster et al. [35], aims to perform minimally invasive laser osteotomy.

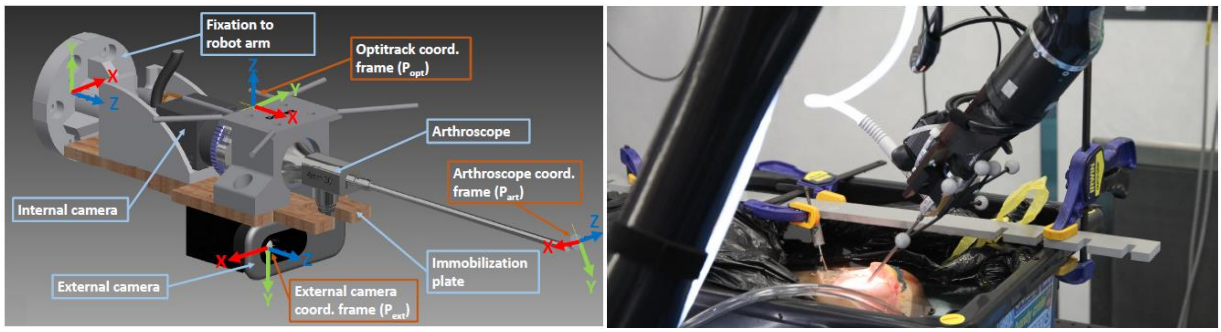

(a) (b)

Fig. 4. (a) The coordinate system of the SLAM external camera mount in Marmol et al.[3], from whose components one can derive the localization of the arthroscope. (b) A tangible model of the system imaging a human limb.

1.3.2 Computer vision

From segmentation to adaptive light control, computer vision of the surgical field is vital to achieving fully autonomous KA, and helpful in assisting surgeons in semi-robotic KA. Though research in computer vision has not been applied to clinical practice, it has shown feasibility to be integrated into modern robotic surgical platforms; such should be the goal of future innovations.

An application that would see great benefit of computer vision is ACL reconstruction, as identifying the placements of femoral and tibial tunnels relative to meniscus and cartilage is integral to more anatomic treatment and satisfactory clinical outcomes. Past research has seen segmentation of knee cartilage from ultrasound (US) images using Mask Regional Convolutional Neural Network (CNN), where images are preprocessed and the network is trained with the COCO 2016 dataset [38]. Segmentation of other intraarticular structures is achieved through deep learning, particularly the UNet architecture [39, 40]. Moreover, multi-pose imaging is made possible by homogeneous transformations between MRI of the knee at various angles[41], and

4D US which can generate a volumetric atlas [42]. From this, Antico et al. presents a Bayesian CNN for segmentation of femoral cartilage, where the algorithm can return both the probability of a pixel being part of the target structure and the confidence with which the CNN reaches such a conclusion [43]. Autonomous KA, whether partially or fully, greatly benefits from identifying important anatomical landmarks, given the poor intraarticular vision from which surgeons suffer intraoperatively. Researchers ought to continue to develop datasets and train networks to detect knee structures with greater accuracy and precision, as well as pave the way for this technology to be used in the operating room.

Algorithms can also be utilized to enhance the arthroscopic image of intraarticular structures. For example, Ali et al. explore the feasibility of support vector machines to determine under- or over-exposure of knee anatomy in stereo arthroscope frames, which enables adaptive lighting [44]. Image enhancement techniques are also discussed in Banach et al., where contrast between different anatomical features is increased for better computer tracking in feature-poor environments [45]. Furthermore, to remove the distortion present in images recorded by endoscopic lens, Barreto et al. publish a camera calibration method using a planar chess grid, improving the practitioner's perception and navigation skill inside the knee joint [46]. Such advancements facilitate KA in that surgeons do not have to manually adjust lighting nor rely on subpar arthroscopic recording, at the cost of little overhead time. Computer vision benefits both autonomous navigation and human perception, and is crucial to future progress in robotic KA.

1.4 Needs and challenges

There are needs and challenges present in both robotic surgery and conventional KA. They may stem from the minimally invasive nature of the procedure or surgeons' reluctance to adopting new technologies. It is thus crucial to consider these setbacks and aim to counter them through innovative methods, boosting the likelihood that such solutions would be accepted and implemented in surgical routines.

Past research has shown surgeons' hesitation to fully endorse robots in the OR. Jaiprakash et al. [47] collect survey responses from a group of Australian orthopedic surgeons, which see only 40.9% of surgeons thinking real-time 3D models would improve visualizations, and only 47.3% of surgeons see semi-robotic devices taking part in future operations, despite the many challenges faced in conventional KA. A change in attitude towards robotic surgery is needed to further integrate newer technologies into these procedures. Moreover, surgeons who do adopt semi-robotic devices in their work are recommended to be thoroughly supported. A realist interview study by Randell et al. [48] suggests having a dedicated robotics team, sufficient equipment and facilities, plenty of training and motivation, and cohesive teamwork. The reward is grand: the long learning curve of 170 procedures to reach baseline competency level in KA [49] can be cut short, for the technology mentioned above can assist with many intraoperative maneuvers.

In addition, conventional KA suffers from human error. Surgeons believe that this procedure entails a long learning curve and high occurrence of iatrogenic, or unintended, cartilage damage [47]. Overestimation of the gap through which to insert an instrument is also common, while surgeons have to continuously change the knee flexion angle for better access to

target anatomy [50]. This contributes to the poor ergonomics of KA, alongside inflexible instruments, physical and cognitive strain, and visibility challenges. Opie et al. show the many tasks a surgeon needs to tend to during the procedure, including changing instruments, redirecting gaze towards different sources of information, and manipulating the patient's leg [12]. Having technology to assist with these tasks not only lightens the load on the surgeon, but also reduce the number of surgeons needed for each procedure. Human error can be minimized using supportive structures such as a leg manipulator [51], or computer algorithms to measure the instrument gap from stereo arthroscopic recording [50]. Ideal assistive devices should still leave the surgeon with plenty of control over the procedure and allow a flexible approach tailored to each patient. These are the needs and challenges of robotic surgery and conventional KA, which are to be alleviated by human-centered design and innovation.

1.5 Innovation and approach

Though many assistive devices are available to aid surgeons, the poor ergonomics of KA remains a problem to be solved. The aim is to develop a device which can provide stable support of the surgeon's apparatus. It would provide all the degrees of freedom associated with conventional KA and preserve the surgeon's autonomy during the procedure, only performing its main function when activated. It would also not be too intrusive of the working space, granting the working tool its full range of motion – axial translation and 3D angles, plus small translations in the plane of the incision, constrained by the circumference of the incision.

Ease of use is emphasized throughout the design process. Surgeons have enjoyed working with simple mechanisms such as the Parallel Portal (Stryker® Endoscopy) [52] and various leg holders [53], which serve to decrease human fatigue and error. If tasks such as

holding the arthroscope can be left to semi-robotic devices, surgeons can focus more on the more crucial tasks, such as observing the arthroscopic recording, maneuvering the working tool, and changing the knee flexion angle. Moreover, the mechanism suspending the arthroscope can provide a stable camera feed, eliminating the effect of hand tremors if the surgeon were to manually wield the arthroscope.

Specifically, the clamping must deform supporting structures enough so that the scope may be clamped, yet such deformations must be elastic. Moreover, the clamping force must result in a friction force large enough to resist sliding motion of the scope. This supporting structure, interacting directly with the arthroscope, may be called the end-effector. The rest of the device focuses on a secure fitting onto the patient's tibia, while promoting the convenience of the surgeon before, during, and after the procedure. This innovation and approach have led to the selection of materials listed in the Methods section.

2. Methods

2.1 Design

The device takes inspiration from other products already prevalent in orthopedics. One of them is a shin pad for protection of the tibia during contact sports. Its rigidity and fit well suit the purpose of protecting the player while not inflicting on their comfort. The other one is a knee brace for post-operation rehabilitation. Its straps help secure the device onto the patient's knee and protect against excessive varus and valgus stress. The widespread use of the shin pad and the knee brace outside of the operating room naturally raises the question if one can find them useful in it. The device developed here demonstrates that with a few adjustments, they can be made into a sturdy mechanism for support during knee arthroscopy.

The design requirements focus on preserving the full workspace found in conventional knee arthroscopy. Mor found this workspace to be characterized by a cone with an included angle of 120 degrees [54]. In the case of a ball joint, the design parameters are, then, as follows:

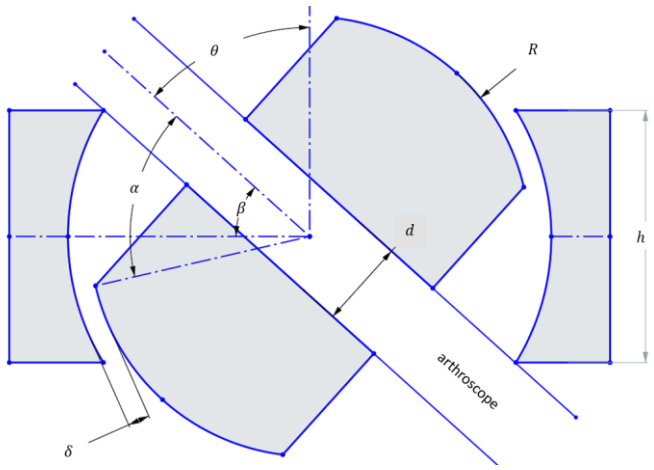

Fig. 5. Geometric parameters of a ball joint used for calculation of the maximum rotation angle which can achieve the 120°- included-angle conical workspace set as a design requirement (126° included angle is a 1.05 design factor)

Table 1. Defined parameters to be used for workspace fulfillment.

Parameter	**Description**	**Value**
δ	Clearance between ball and housing	0.15 mm
θ	Half of the maximum included angle of conical workspace	63º
R	Radius of ball	10 mm
d	Diameter of arthroscope	4 mm
h	Height of housing	To be found

From Fig. 5, one can see that:

$$\beta = 90° - \theta \qquad [1]$$

And,

$$\alpha = \arccos\left(\frac{h/2}{R}\right) \qquad [2]$$

At the maximum θ, the arthroscope collides with the edge of the housing. Then,

$$R\,sin\,\alpha + \delta = \frac{d/2}{cos\,\theta} + \frac{h/2}{tan\,\beta} \qquad [3]$$

Using the design parameters from Table 1, and the above formulas, one can use a numerical solver to get the value of h. Here, the numerical solver SymPy is used.

$$h = 5.47mm \qquad [4]$$

This ensures that the maximum angle to the vertical created by the scope is sufficient to replicate the workspace present in conventional knee arthroscopy, plus a design factor of 1.05 to account for the center of motion not being at the incision, but rather at the ball joint. The surgeon limits this difference in center of motion by placing the ball joint as close to the incision as possible. On the other hand, dimensions not needed for workspace fulfillment are the through-hole diameter and the height of the ball. Firstly, to facilitate the insertion and removal of the

arthroscope through the ball joint, the diameter of the through-hole is selected to be 4.4 mm, which is 0.4 mm greater than the diameter of the scope. Secondly, the height of the ball is chosen to be 16 mm, so that the inner clamp surface may make contact with the ball for most angles to the vertical, and enough space is left for deformed structures to occupy, and enough thickness is given to structures so that they may not fracture. The dimensions of the slits may be seen in Fig. 6 below.

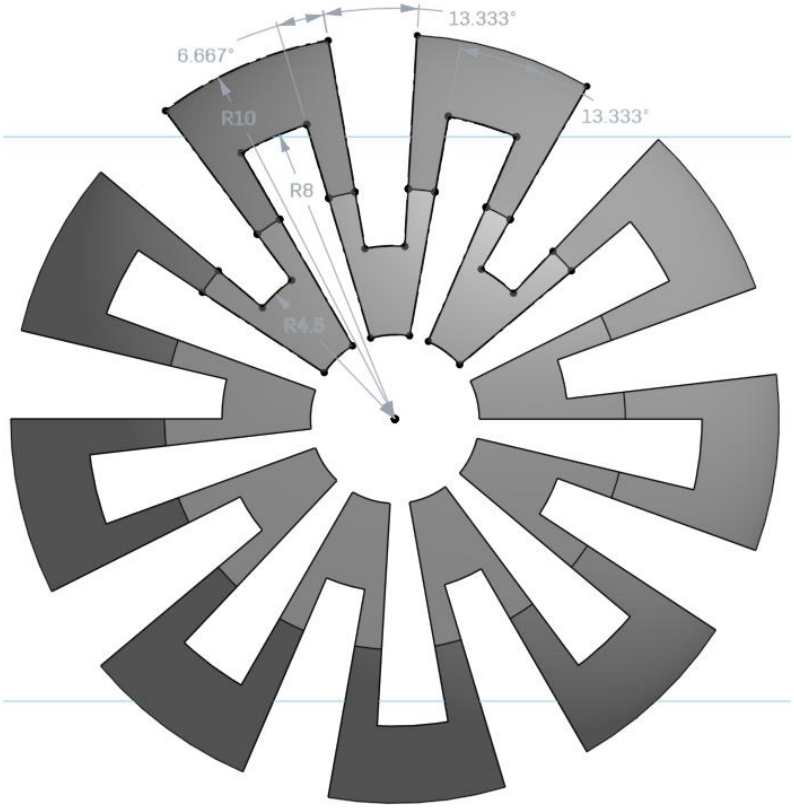

Fig. 6. Dimensions of the slits made in the ball joint.

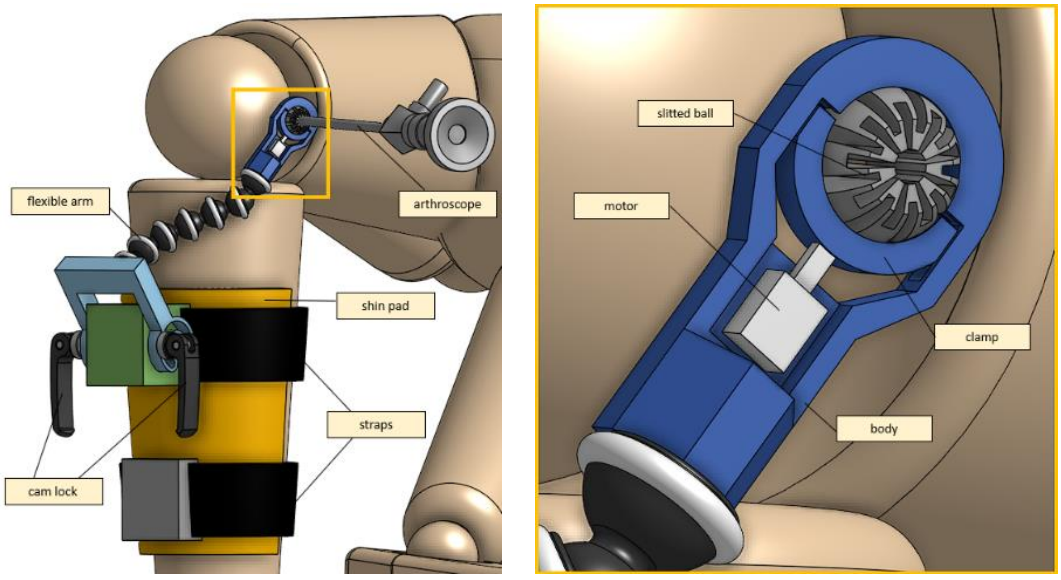

Fig. 7. left - Overall components of device to be fitted on patient's injured, operative leg. right – Components of miniature braking system for tool suspension (the end-effector).

The overall device makeup is shown in Fig. 7. Some components are readily available to be purchased, such as cam locks and flexible arm. Others are custom-made and 3D printed, such as the end-effector assembly minus the motor. Adapters, seen in green and gray, are rigidly attached onto the shin pad, through which straps go for securing the pad onto the shank. Cam locks are used to restrict the motion of the crank, which can rotate freely when cam locks are not clamping. Screw threads are present on both ends of the flexible arm, so brass inserts are used to connect the flexible arm with the crank and the end-effector body.

In the end-effector assembly, grooves are designed into the body so that the clamp does not fall out of place and can only travel in the clamping direction. The motor is any device which can provide a clamping force towards the slitted ball. As seen in prototyping below, the motor is chosen to be a miniature air cylinder.

2.2 Finite element analysis

The point of interest for finite element analysis is the stress and deformation of the ball joint when under clamping force without the arthroscope inserted, and the force which resists the arthroscope sliding along the ball through-hole when clamping is activated with the scope inserted. Abaqus is the program chosen to run the simulations for this analysis. After the design has been made in Onshape, an ACIS file is downloaded and imported into Abaqus. Then, the part is assigned a material, which is polyethylene, with its corresponding mechanical properties shown in Table 2. To mesh the components, the clamp is given a hex mesh of size 1 mm, the ball a hex mesh of size 0.8 mm, while the body is given a tet mesh of size 1 mm.

Table 2. Mechanical properties of selected material - polyethylene

Density	950 $kg \cdot m^{-3}$ [55]
Young's modulus	0.70 GPa [55]
Poisson ratio	0.46 [56]
Coefficient of friction between polyethylene and polyethylene	0.2 [57]
Coefficient of friction between polyethylene and stainless steel	0.2 [57]

2.2.1 Without arthroscope inserted

The simulation is first run without the arthroscope through the ball, and maximum deformation of the slitted ball is recorded at various angles to the vertical. After meshing, loads and boundary conditions are defined to be as realistic as possible. To demonstrate the compressibility of the ball joint and model the clamping of an actuator, a concentrated force of 10 N is applied at the center of the clamp in the clamping direction, which is the negative y-direction in Fig. 8. Boundary conditions for this analysis are listed in Table 3 and also graphically shown in Fig. 8.

Abaqus is set to detect general contact between parts, with contact properties between certain surfaces specified by their matching coefficient of friction listed in Table 2. For every simulation, the "Dynamic, Explicit" package is used, precision is set to "Double – analysis + packager", and Nodal output precision is set to "full". Starting from the ball making a 0º angle with the vertical, the simulation is repeated for every 10º turned in the xz-plane, with the axis of rotation as the negative x-axis following right-hand convention (refer to Fig. 8).

Table 3. Boundary conditions for ball deformation testing without arthroscope.

Type	Placement	Purpose
Encastre – full constraint on all degrees of freedom	Hole at end where a brass insert is meant to be attached	Ball joint assembly is screwed onto the flexible arm
Limited to one-dimensional motion in the y-axis	Center of clamp, assumed to be where actuator attaches to clamp	Actuator may only move clamp along this axis

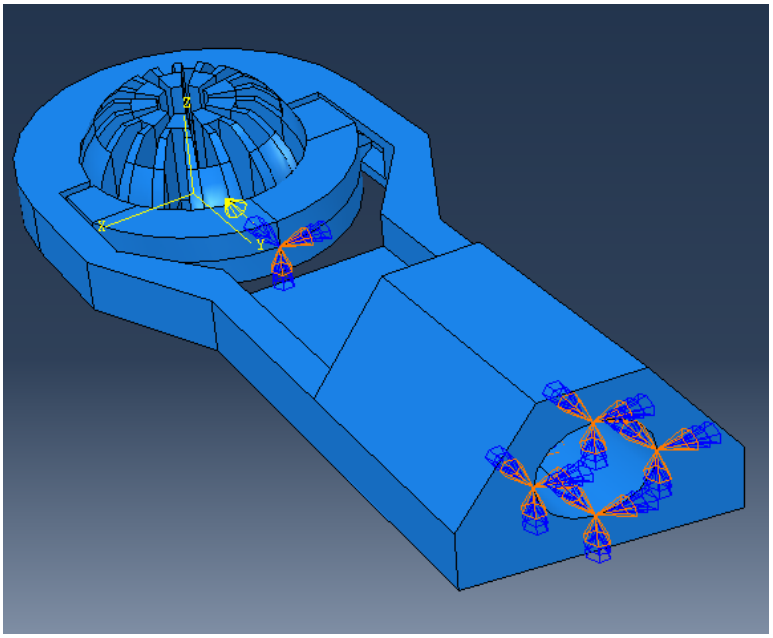

Fig. 8. Load (10N) and boundary conditions where arthroscope is not inserted.

2.2.2 With arthroscope inserted

Next, the more realistic situation is tested, where ball deformation is observed with the arthroscope inserted into the through-hole. In Abaqus, a 20-mm long cylinder with diameter 4 mm is made to represent a section of an arthroscope. Then, this section is given a hex mesh of size 0.8 mm is placed through the ball joint. The outer surface of the section is assigned to be stainless steel, with general contact between the clamp and the section defined with a friction coefficient of 0.2 (see Table 2).

For this simulation, the analysis is divided into two steps. In step 1, the ball is compressed under the applied load, until it fully clamps the arthroscope inside and reaches dynamic equilibrium, with a step time of 0.5. In step 2, full clamping is left activated from step 1, the top node of the section is assigned a linear displacement of constant velocity in the positive

z-direction (refer to Fig. 8), with a step time of 1.0. The said displacement has a “Tabular” amplitude, which is 0 at step time 0, and 4 at step time 1. Because of the sufficient length of the cylindrical section, the displacement has a “Tabular” amplitude, which is 0 at step time 0, and 4 at step time 1during step 2.

Here, the goal is to record how much reaction force in the direction along the through-hole prevents the scope from sliding during clamping. Boundary conditions are like those used in previous testing without the arthroscope, with the addition of a displacement of the cylindrical section, all of which are listed in Table 4. Fig. 9 shows the load applied and boundary conditions used in this instance.

Just as in the previous analysis without the arthroscope inserted, the “Dynamic, Explicit” package is used, precision is set to “Double – analysis + packager”, and Nodal output precision is set to “full”. In all test cases, the ball is vertically oriented. Results are recorded for all combinations of clamping forces of 5, 10, 15, and 20 newtons; and friction coefficients of 0.2 and 0.3.

Table 4. Boundary conditions for analysis with arthroscope

Step	**Type**	**Placement**	**Purpose**
1, 2	Encastre – full constraint on all degrees of freedom	Hole at end where a brass insert is meant to be attached	Ball joint assembly is screwed onto the flexible arm
1, 2	Limited to one-dimensional motion in the y-axis	Center of clamp, assumed to be where actuator attaches to clamp	Actuator may only move clamp along this axis
2	Displacement of arthroscope along hole direction	At end of cylindrical section representing a scope	Model the scope sliding along hole direction

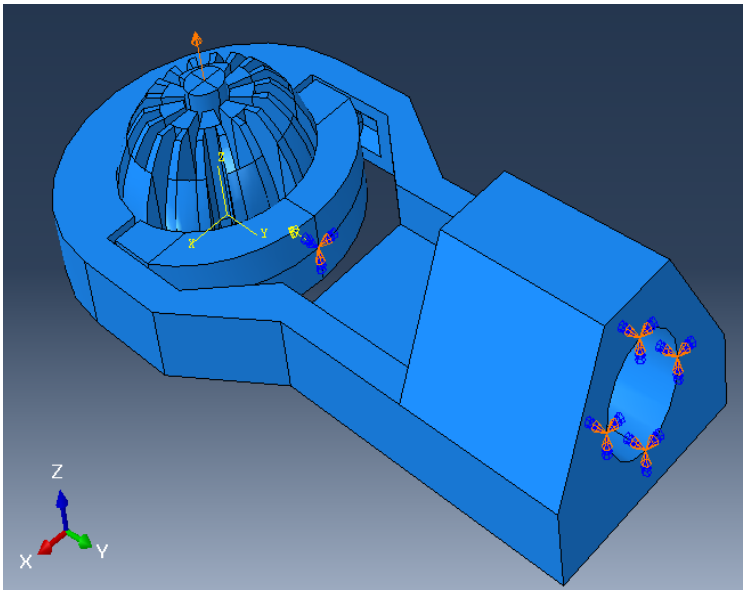

Fig. 9. A 10N load is applied to clamp and compress the ball joint, and all boundary conditions defined on the model during the simulation with scope inserted.

2.3 Prototyping

After the design and FEA processes suggest a potentially feasible piece of hardware, prototyping is the next step in fabricating the device. First, custom-made parts are exported as an STL file from Onshape. Using PrusaSlicer, the models are sliced and the G-code for printing them is generated. They are then 3D printed using an Ender-3 (Creality®) with PLA as the filament. To avoid printing unnecessary support structures for overhangs, such protruding features are designed to rise at a 45 angle to the horizontal, which can be seen in Fig. 10. To summarize, Fig. 11 shows the interface of PrusaSlicer and how the end-effector assembly is printed.

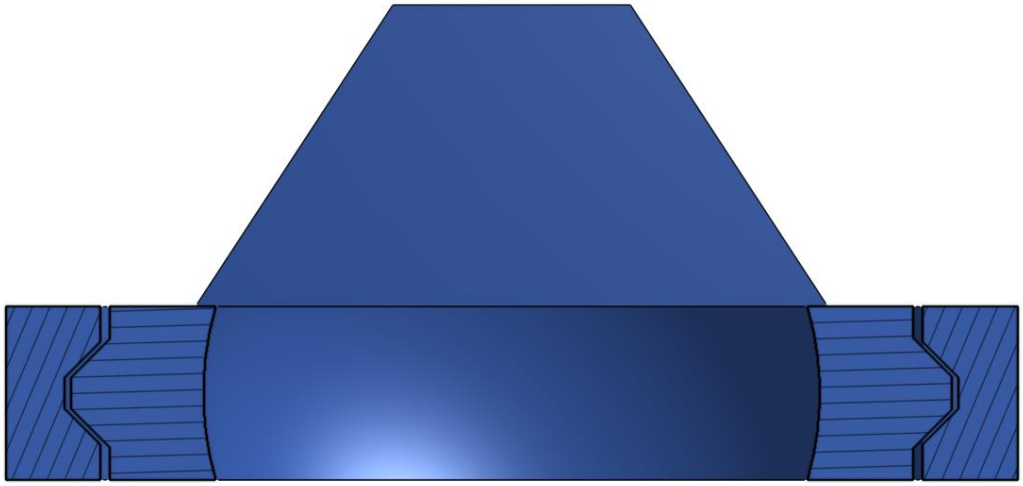

Fig. 10. Cross-section of the ball joint assembly at the interface between the clamp and the body.

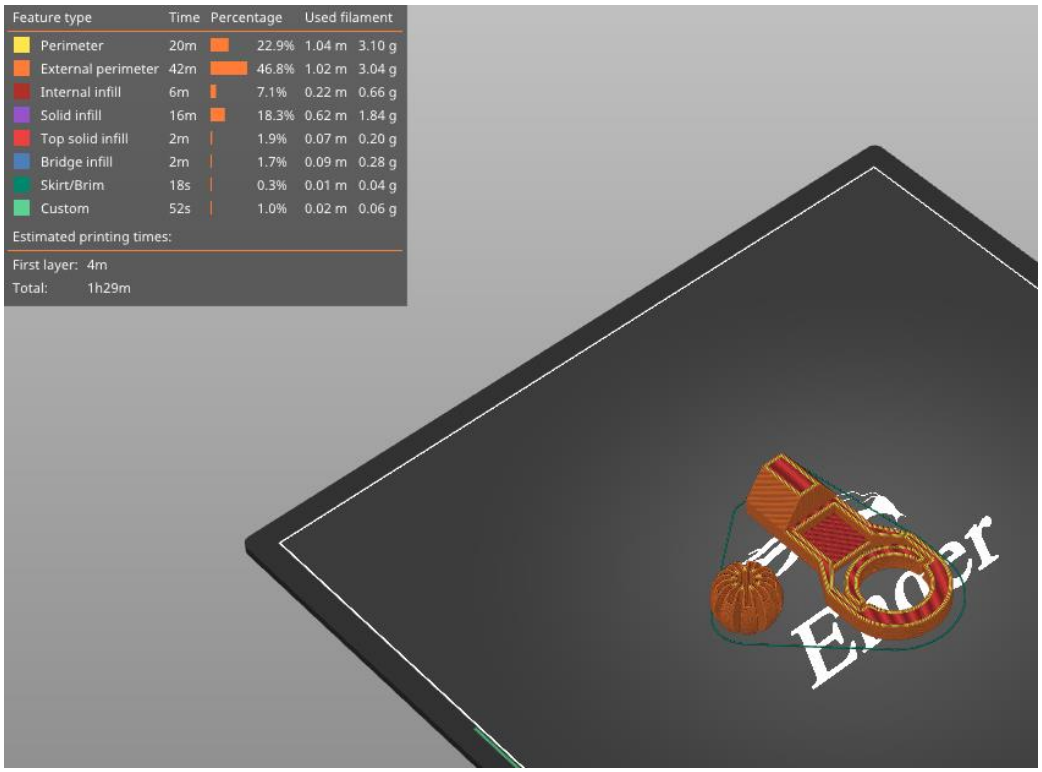

Fig. 11. PrusaSlicer interface and the orientation of the printed parts. The bottom of all features is seen to lay flat on the printing bed. The clamp is printed at its intended location, while the ball is printed outside of it.

3. Results

3.1 Finite element analysis

3.1.1 Without arthroscope inserted

Here, the Abaqus FEA simulation results for each ball orientation is presented. One instance of the von Mises stress and deformation in the ball joint assembly is shown in Fig. 12a and Fig. 12b, respectively. Moreover, the maximum deformation recorded at each ball angle under clamping are reported in Fig. 13.

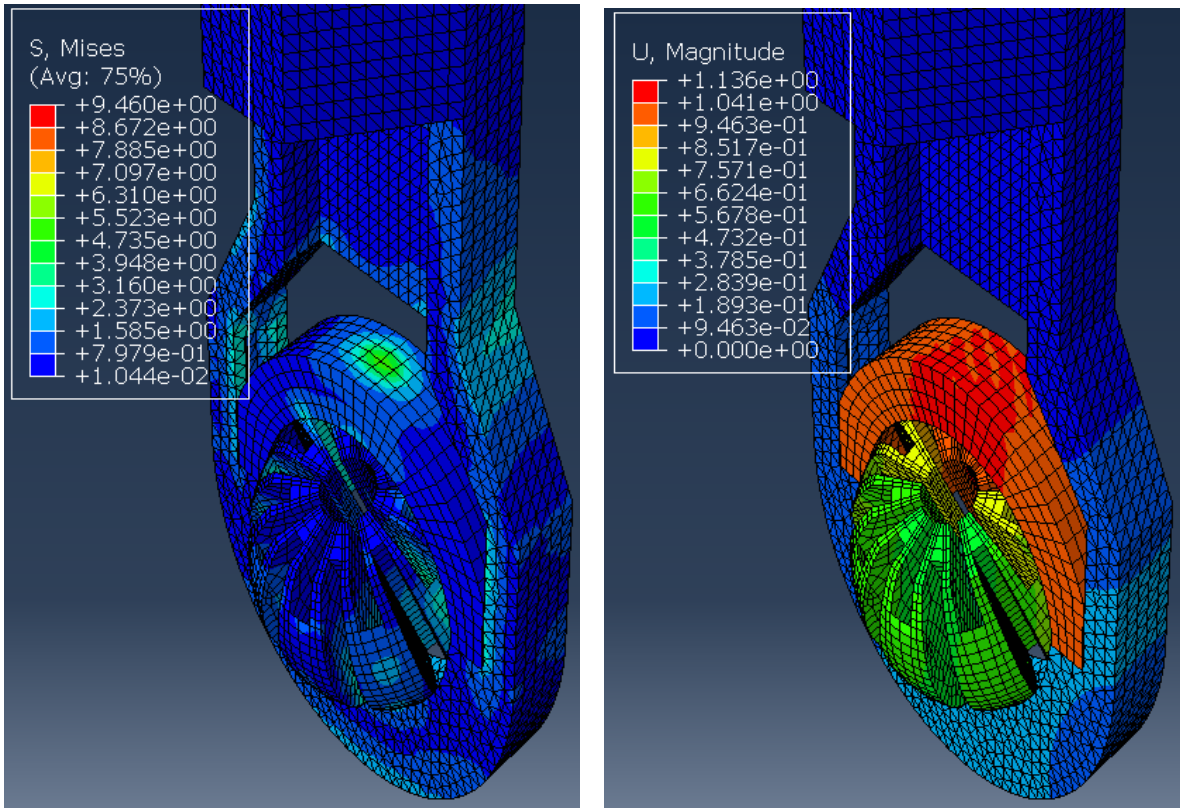

(a) *(b)*

Fig. 12. The ball inside the housing is turned 60º to the vertical and applied a clamping force. (a) The von Mises stress observed in MPa; (b) The deformation observed in mm.

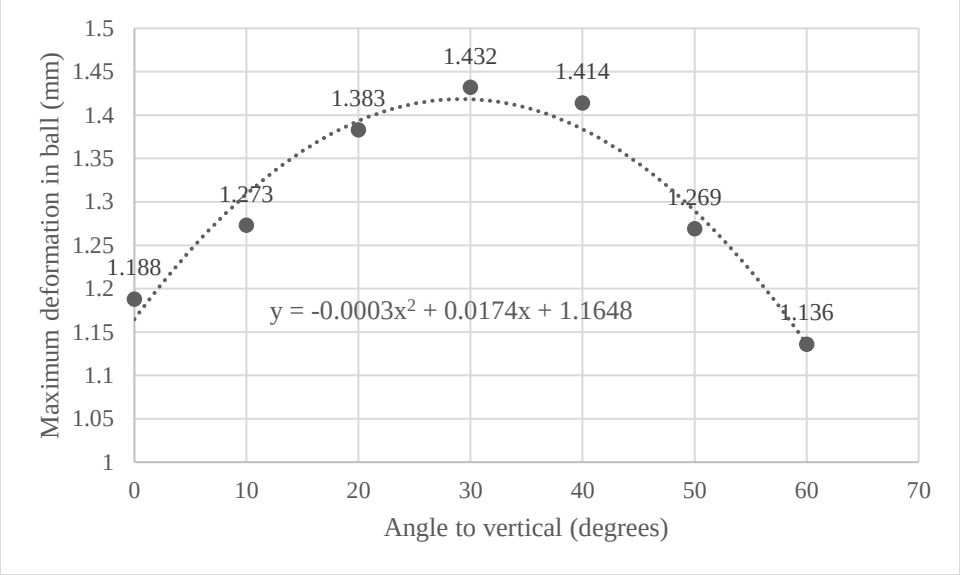

Fig. 13. Maximum deformation observed in slitted ball joint at various angles to the vertical.

3.1.2 With arthroscope inserted

Next, the structural analysis with the arthroscope inserted is examined, where step 1 in the case of 10 N clamping force is graphically illustrated in Fig. 14. Furthermore, Fig. 15 shows the contact forces in the positive z-direction between the arthroscope and inner surfaces of the slitted ball, as the arthroscope is pulled upwards with a friction coefficient of 0.2. The von Mises stresses occurring in the ball joint assembly during full clamping after step 1 is reported in Fig. 16, where the maximum stresses are listed for each clamping force. One may also be interested in the mean of the contact forces over time for each clamping force, and this is demonstrated in Fig. 17 (since meaningful values of contact force are those occurring during step 2, only those values are included in the calculations). Fig. 18 compares contact forces in the same manner as Fig. 15, but with the friction coefficient of 0.3. And finally, one can see the increase in contact

forces due to an increase in friction coefficient in Fig. 19, as the contact forces under 5 N of clamping force is shown for friction coefficients of both 0.2 and 0.3.

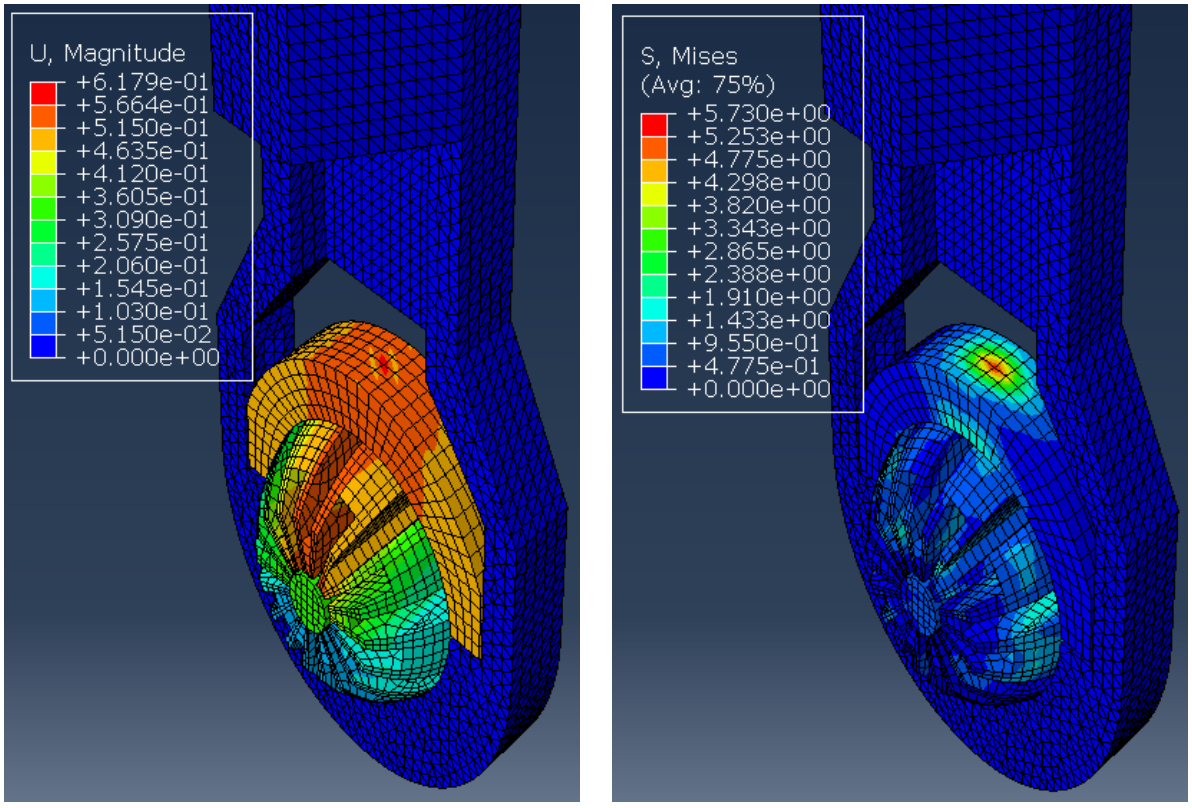

(a) *(b)*

Fig. 14. The ball inside the housing has a cylindrical section inserted and applied a clamping force. (a) The von Mises stress observed in MPa; (b) The deformation observed in mm.

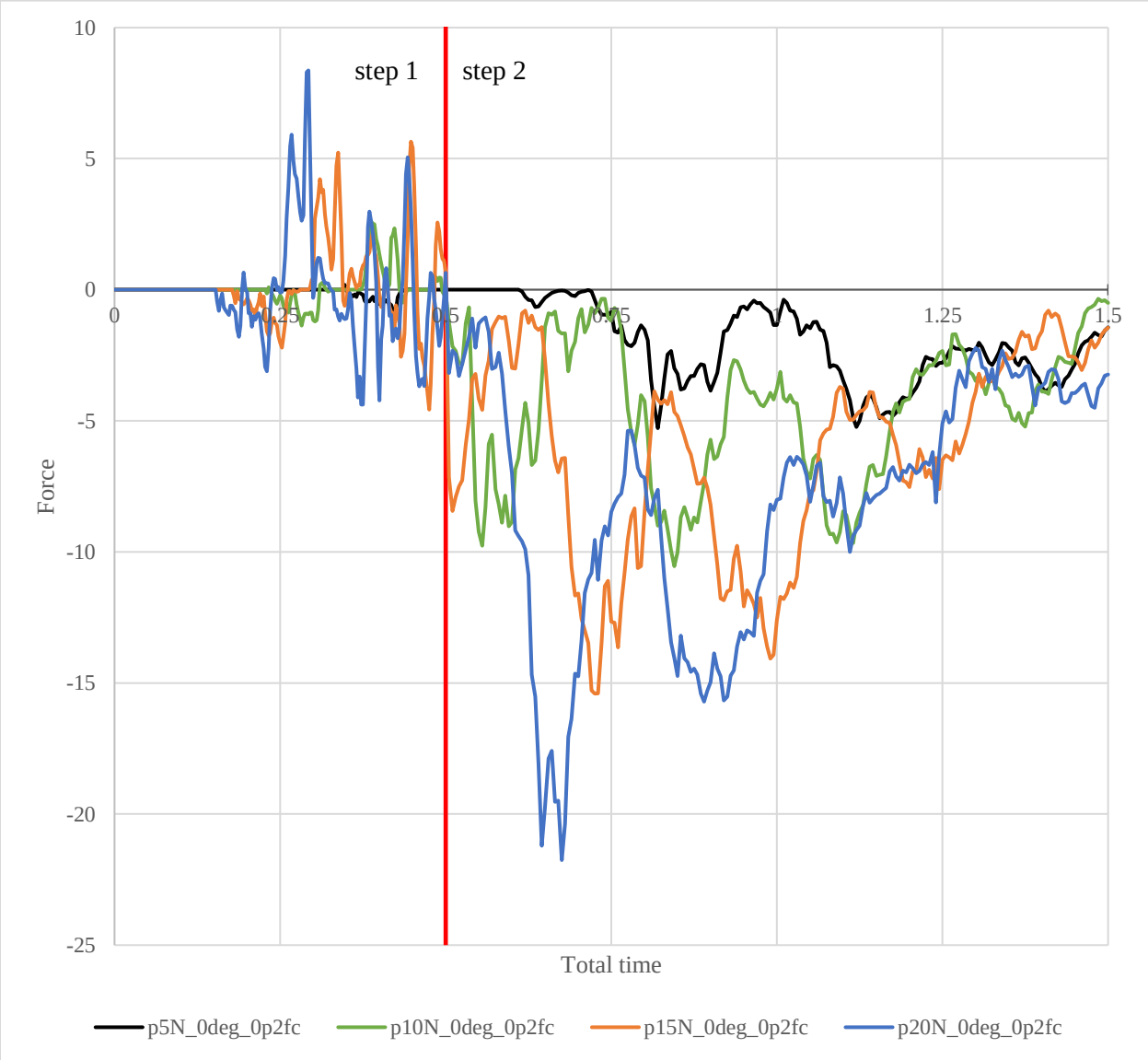

Fig. 15: Contact force (N) measured in the positive z-direction between the arthroscope and the inner surfaces of the deformed ball, where friction coefficient is 0.2.

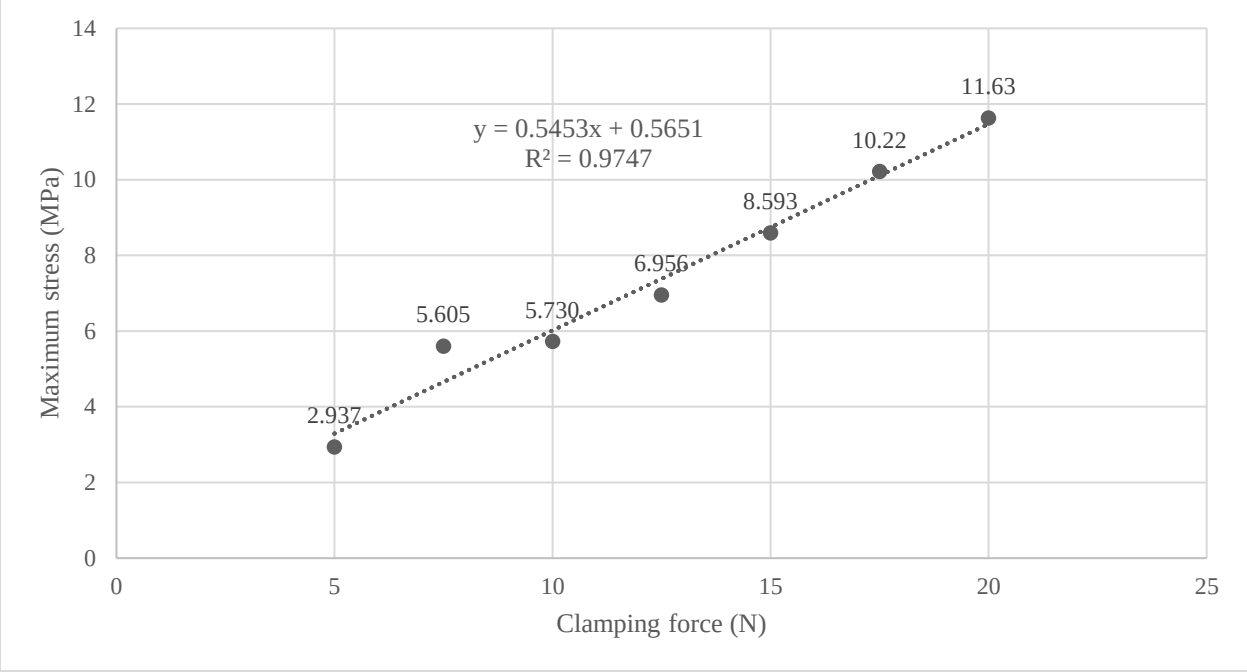

Fig. 16. The maximum von Mises stress occurring in the ball joint assembly for each clamping force, where the ball is vertically oriented.

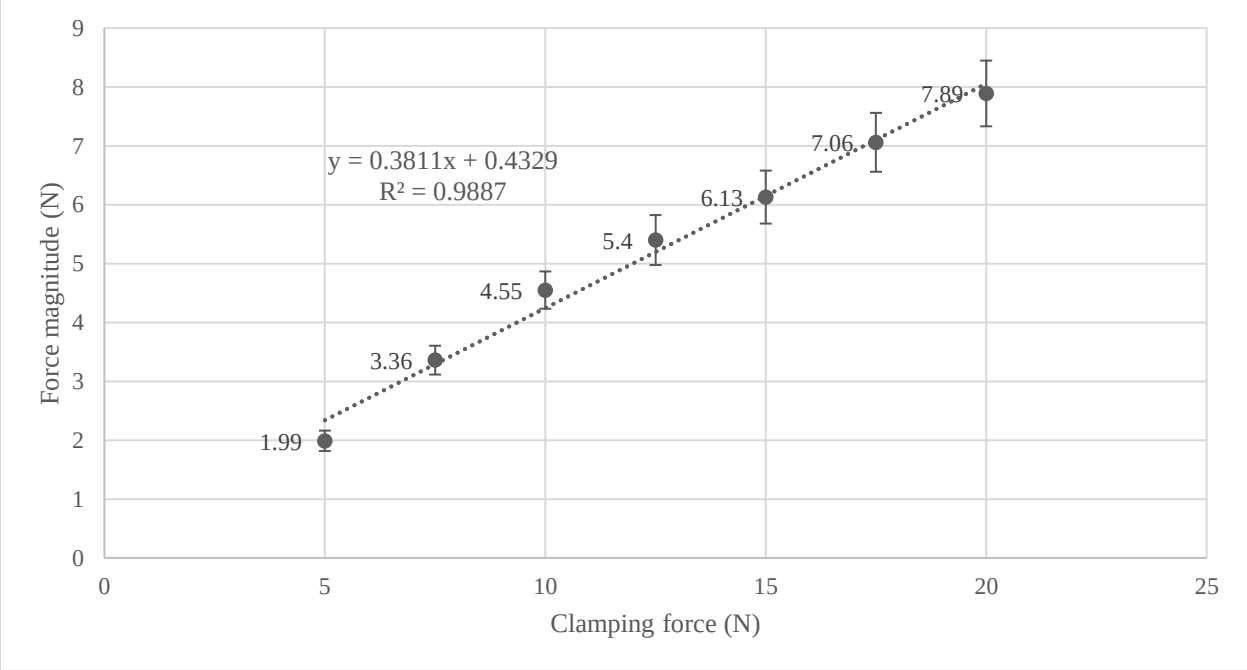

Fig. 17. Mean contact force for each clamping force and their respective 95% confidence interval for true mean.

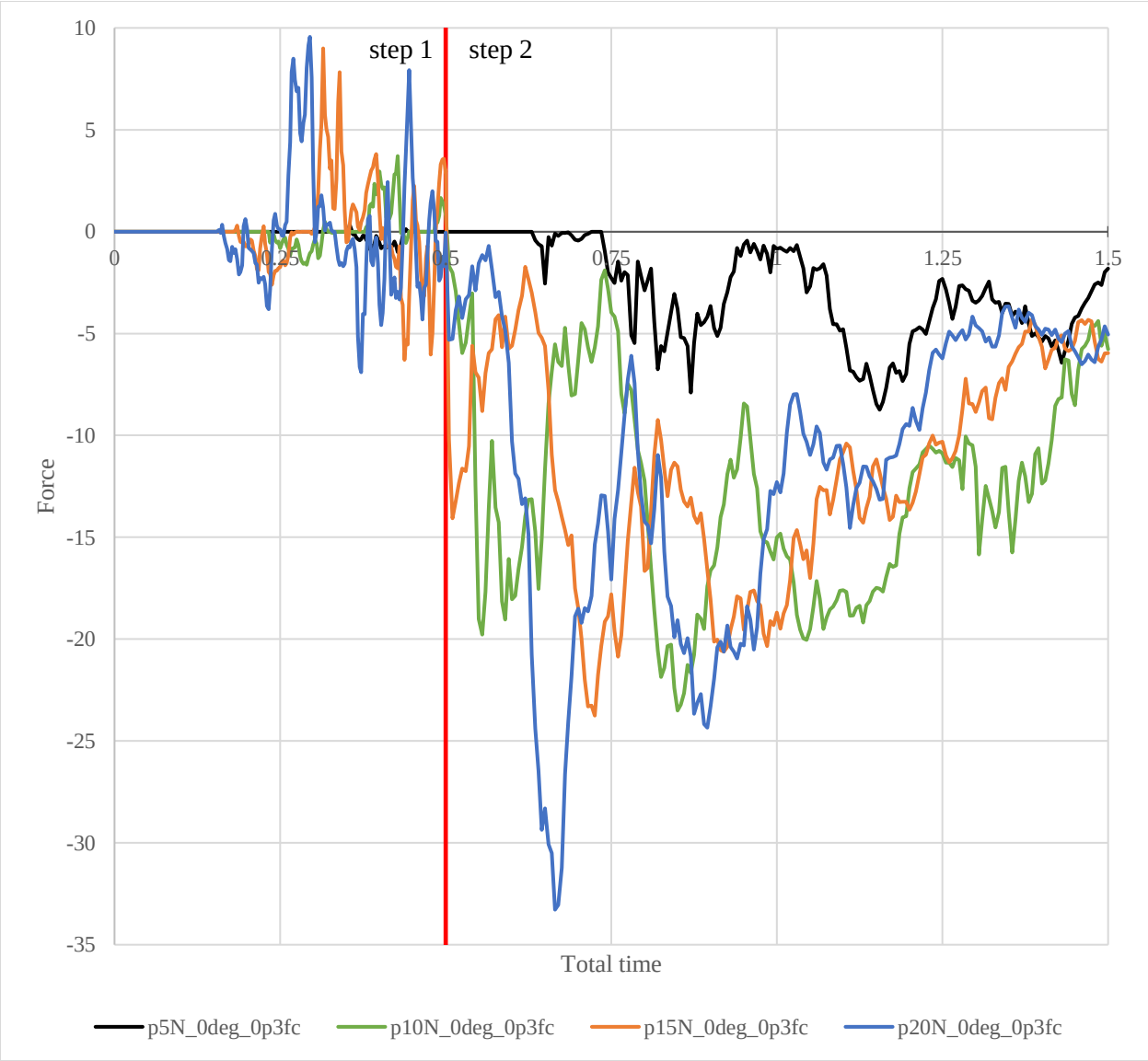

Fig. 18: Contact force (N) measured in the positive z-direction between the arthroscope and the inner surfaces of the deformed ball, where friction coefficient is 0.3.

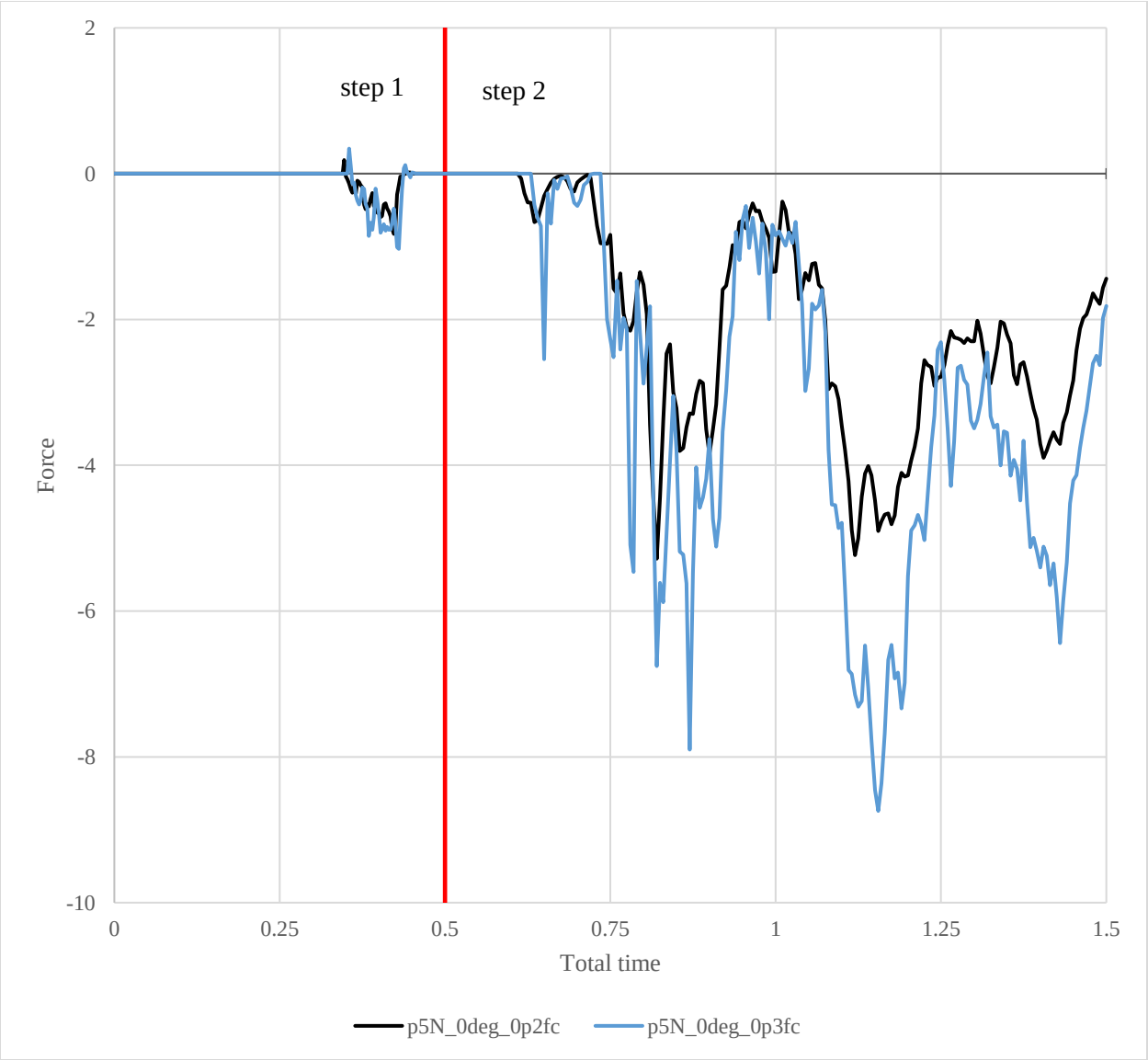

Fig. 19. Contact forces under 5 N of clamping force with friction coefficients of both 0.2 and 0.3.

3.2 Prototyping

Though the device comprises of many components, the most vital piece is the slitted ball joint assembly. Fig. 20 shows the ball joint assembly specifically, though without an actuator to provide the clamping force. Nonetheless, when clamping force is present, the profile of the center perimeter becomes an ellipse whose minor axis is aligned with the clamping direction, consistent with the deformed result computed by FEA (see Fig. 11).

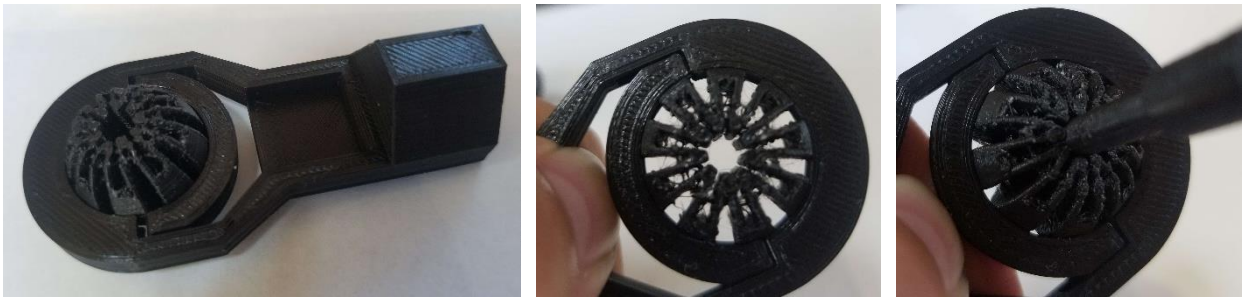

(a) *(b)* *(c)*

Fig. 20. (a) The 3D-printed rod end using PLA; (b) Deformation of the slitted ball with clamping force applied without the scope; (c) Deformation of the slitted ball with clamping force applied with the scope

4. Discussion

4.1 Ball joint assembly

The ball joint assembly exhibited desirable compressibility to be used for arthroscope clamping. Polyethylene is chosen to be the material whose properties are used in the FEA simulation because of its wide usage as a thermoset plastic. Its yield stress of 19 MPa [58] is also greater than the stresses incurred during clamping in the ball joint assembly (see Fig. 16). Hence, it may be selected as a material used to make the presented ball joint assembly.

It is worth noting the following trends in the contact forces graphs shown above. In step 1, fluctuations in contact force are due to the inner surfaces of the ball touching the arthroscope and pushing it against the other side of the ball. These values are insignificant in finding the force resisting the scope from sliding. In step 2, the results are as expected. In Fig. 15, the maximum contact force magnitude increases as the clamping force increases. As the arthroscope section keeps being displaced, the contact forces gradually decrease. The same trend is shown in Fig. 18, though the results are greater in magnitude due to the greater friction coefficient which is expected. One case of this is also confirmed in Fig. 19, where the contact forces under 5 N clamping for both 0.2 and 0.3 friction coefficient are compared.

Also of interest is seeing how the von Mises stress and mean contact force change with increasing clamping force. Fig. 16 shows that the maximum von Mises stress observed is positively correlated to the clamping force, and none of them exceed the 19 MPa yield stress limit. In Fig. 17, the magnitude of the mean contact force positively correlates with the clamping force, and so does the standard deviation of contact forces under each clamping force.

4.2 Future research

Further testing of the device is needed. In computer analysis, more realistic loading conditions may be tested by seeing how the assembly withstands external torque on the arthroscope, or how different weights of the arthroscope may strain the assembly. The contact friction force computation above may also be tested in real life by using a load cell to pull the arthroscope along the through-hole under clamping, after the clamping mechanism will have been designed. Through this, one seeks to compare computer-generated results to experimental testing, which helps to certify whether the feasibility shown here is realistically true.

Before the device is ready for use in the operating room, there are more aspects which it must fulfill. Firstly, a safety mechanism must be present in case the surgeon cannot disengage clamping electrically. This situation is dangerous in that the arthroscope cannot be removed from the patient's knee in a safe manner, and forcefully pulling the arthroscope out may result in inadvertent damage to intraarticular structures. Such a safety mechanism must be physical, most importantly, and straightforward for surgeons to carry out. It also must not impede the original function of the clamping force on the ball joint assembly, and not require excessively forceful measures which may damage the patient's knee. Secondly, feedback from surgeons on how to improve the device is greatly needed. The proof-of-concept prototype is planned to be presented to collaborators at the UCF College of Medicine at Lake Nona for advice on how to better adapt the device to the actual procedure. Though the functionality may be guaranteed, it is crucial to ensure that surgeons view the device as a positive contribution to their work, facilitating the procedure without obstructing routine practices.

Another future goal is to make the device more suitable for surgical use. Due to the anisotropic structure of 3D-printed PLA, it is hard to predict accurately and consistently the resulting deformation. The final product, to be used in surgery, needs to be smooth, burr-free, nonabsorbent, and homogeneous. Therefore, injection molding may be more appropriate than additive manufacturing in fabricating the final product. The same applies for other components of the device, like the crank and shin pad. Instead of having adapters for the shin pad to connect with the crank, the shin pad can be designed with such adapters and injection molded. All components, including the clamping mechanism, will need to be safe for use during surgery.

5. Conclusion

The ball joint assembly is tested as part of a semi-robotic device for knee arthroscopy, where a tool inserted into the through-hole of the ball joint is clamped and suspended. The whole assembly was successfully printed using additive manufacturing as a prototype. Abaqus FEA simulation shows that the maximum von Mises stress and the magnitude of contact forces positively correlates with the clamping force, where the stress incurred is still in the elastic range of polyethylene (the material selected). Future research will focus on implementing the actuator into the ball joint assembly and developing a safety mechanism for the device, as well as gathering feedback from surgeons to better adapt it to surgical use.

6. References

1. Kim, J., et al. *Development and Preclinical Trials of a Novel Steerable Cannula for 360° Arthroscopic Capsular Release in Minimally Invasive Surgery*. in *2020 42nd Annual International Conference of the IEEE Engineering in Medicine & Biology Society (EMBC)*. 2020. IEEE.
2. Yan Nai, T., J.L. Herder, and G.J.M. Tuijthof, *Steerable Mechanical Joint for High Load Transmission in Minimally Invasive Instruments.* Journal of Medical Devices, 2011. **5**(3): p. 034503.
3. Marmol, A., P. Corke, and T. Peynot. *ArthroSLAM: Multi-Sensor Robust Visual Localization for Minimally Invasive Orthopedic Surgery*. in *2018 IEEE/RSJ International Conference on Intelligent Robots and Systems (IROS)*. 2018.
4. Jackson, R.W. *From the scalpel to the scope: the history of arthroscopy*. in *Baylor University Medical Center Proceedings*. 1996. Taylor & Francis.
5. McKeon, B.P., J.V. Bono, and J.C. Richmond, *Knee arthroscopy*. Vol. 578. 2009: Springer.
6. Phillips, B.B., *General principles of arthroscopy.* Campbell's operative orthopaedics, 2003. **3**: p. 10.
7. Vitiello, V., et al., *Emerging Robotic Platforms for Minimally Invasive Surgery.* IEEE Reviews in Biomedical Engineering, 2013. **6**: p. 111-126.
8. Van der List, J.P., H. Chawla, and A.D. Pearle, *Robotic-assisted knee arthroplasty: an overview.* Am J Orthop, 2016. **45**(4): p. 202-211.

9. Girgis, I.E., *Workspace and Kinematic Modeling and Analysis of Semi-Robotic Laparoscopic Surgery.* Honors Undergraduate Theses, 2021. **916**.

10. Taylor, G., et al., *Surgical innovations: Addressing the technology gaps in minimally invasive surgery.* Trends in Anaesthesia and Critical Care, 2013. **3**(2): p. 56-61.

11. Karthik, K., et al., *Robotic surgery in trauma and orthopaedics: a systematic review.* The bone & joint journal, 2015. **97**(3): p. 292-299.

12. Opie, J., et al. *Understanding the challenges and needs of knee arthroscopy surgeons to inform the design of surgical robots*. ACM.

13. Araujo, P.H., et al., *Use of a fluoroscopic overlay to guide femoral tunnel placement during posterior cruciate ligament reconstruction.* Am J Sports Med, 2014. **42**(11): p. 2673-9.

14. Moloney, G., et al., *Use of a fluoroscopic overlay to assist arthroscopic anterior cruciate ligament reconstruction.* Am J Sports Med, 2013. **41**(8): p. 1794-800.

15. Swami, V.G., et al., *Reliability of estimates of ACL attachment locations in 3-dimensional knee reconstruction based on routine clinical MRI in pediatric patients.* Am J Sports Med, 2013. **41**(6): p. 1319-29.

16. Rankin, I., H. Rehman, and M. Frame, *3D-Printed Patient-Specific ACL Femoral Tunnel Guide from MRI.* Open Orthop J, 2018. **12**: p. 59-68.

17. Nakagawa, T., et al., *Intraoperative 3-dimensional imaging-based navigation-assisted anatomic double-bundle anterior cruciate ligament reconstruction.* Arthroscopy, 2008. **24**(10): p. 1161-7.

18. Lee, B.H., et al., *Clinical advantages of image-free navigation system using surface-based registration in anatomical anterior cruciate ligament reconstruction.* Knee Surgery, Sports Traumatology, Arthroscopy, 2016. **24**(11): p. 3556-3564.

19. Plaweski, S., et al., *Evaluation of a computer-assisted navigation system for anterior cruciate ligament reconstruction: prospective non-randomized cohort study versus conventional surgery.* Orthop Traumatol Surg Res, 2012. **98**(6 Suppl): p. S91-7.

20. Modi, C.S., G. Morris, and R. Mukherjee, *Computer-simulation training for knee and shoulder arthroscopic surgery.* Arthroscopy, 2010. **26**(6): p. 832-40.

21. Heng, P.A., et al., *Virtual reality techniques. Application to anatomic visualization and orthopaedics training.* Clin Orthop Relat Res, 2006. **442**: p. 5-12.

22. Li, R. and Y. Lou. *Research and development of the regulation training system of minimally invasive knee surgery based on VR technology*. in *2019 14th International Conference on Computer Science & Education (ICCSE)*. 2019. IEEE.

23. Bjelland, O., et al., *Intraoperative Data-Based Haptic Feedback for Arthroscopic Partial Meniscectomy Punch Simulation.* IEEE Access, 2022. **10**: p. 107269-107282.

24. Yu, Y., et al. *Research and development of virtual simulation teaching system for knee joint anatomy*. in *2020 15th International Conference on Computer Science & Education (ICCSE)*. 2020.

25. Megali, G., et al., *Computer-assisted training system for knee arthroscopy.* The International Journal of Medical Robotics and Computer Assisted Surgery, 2005. **1**(3): p. 57-66.

26. Cowan, J.B., et al., *Computer-Simulated Arthroscopic Knee Surgery: Effects of Distraction on Resident Performance.* Orthopedics, 2016. **39**(2): p. e240-5.

27. Boutefnouchet, T. and T. Laios, *Transfer of arthroscopic skills from computer simulation training to the operating theatre: a review of evidence from two randomised controlled studies.* Sicot j, 2016. **2**: p. 4.

28. Baker, B.E., et al., *Review of meniscal injury and associated sports.* The American journal of sports medicine, 1985. **13**(1): p. 1-4.

29. Mack, M.J., *Minimally Invasive and Robotic Surgery.* JAMA, 2001. **285**(5): p. 568.

30. Fox, A.J.S., A. Bedi, and S.A. Rodeo, *The Basic Science of Human Knee Menisci.* Sports Health: A Multidisciplinary Approach, 2012. **4**(4): p. 340-351.

31. Cui, Z., et al. *Design of a 3-axial force/torque sensor for arthroscopy force sensing*. in *2011 IEEE International Conference on Mechatronics and Automation*. 2011. IEEE.

32. Long, Z., et al., *Real-Time 3D Visualization and Navigation Using Fiber-Based Endoscopic System for Arthroscopic Surgery.* Journal of Advanced Computational Intelligence and Intelligent Informatics, 2016. **20**(5): p. 735-742.

33. Fasel, L., et al. *The SEA-Scope: Torque-limited endoscopic joint control for telemanipulation or visual servoing through tendon force control with series elastic actuation*. in *2021 International Symposium on Medical Robotics (ISMR)*. 2021. IEEE.

34. Kosa, G., et al. *Automation of a Flexoscope for Laser Osteotomy*. in *CAOS 2017. 17th Annual Meeting of the International Society for Computer Assisted Orthopaedic Surgery*. 2017. EasyChair.

35. Eugster, M., et al., *Robotic Endoscope System for Future Application in Minimally Invasive Laser Osteotomy: First Concept Evaluation.* IEEE Transactions on Medical Robotics and Bionics, 2022. **4**(3): p. 621-633.

36. Razjigaev, A., et al., *End-to-End Design of Bespoke, Dexterous Snake-Like Surgical Robots: A Case Study With the RAVEN II.* IEEE Transactions on Robotics, 2022: p. 1-14.

37. Ciszkiewicz, A. and G. Milewski, *Path planning for minimally-invasive knee surgery using a hybrid optimization procedure.* Computer Methods in Biomechanics and Biomedical Engineering, 2018. **21**(1): p. 47-54.

38. Kompella, G., et al. *Segmentation of Femoral Cartilage from Knee Ultrasound Images Using Mask R-CNN*. in *2019 41st Annual International Conference of the IEEE Engineering in Medicine and Biology Society (EMBC)*. 2019.

39. Jonmohamadi, Y., et al., *Automatic Segmentation of Multiple Structures in Knee Arthroscopy Using Deep Learning.* IEEE Access, 2020. **8**: p. 51853-51861.

40. Antico, M., et al., *Deep Learning-Based Femoral Cartilage Automatic Segmentation in Ultrasound Imaging for Guidance in Robotic Knee Arthroscopy.* Ultrasound Med Biol, 2020. **46**(2): p. 422-435.

41. Constantinescu, M.A.M., et al., *Constrained Statistical Modelling of Knee Flexion From Multi-Pose Magnetic Resonance Imaging.* IEEE Transactions on Medical Imaging, 2016. **35**(7): p. 1686-1695.

42. Antico, M., et al., *4D Ultrasound-Based Knee Joint Atlas for Robotic Knee Arthroscopy: A Feasibility Study.* IEEE Access, 2020. **8**: p. 146331-146341.

43. Antico, M., et al., *Bayesian CNN for Segmentation Uncertainty Inference on 4D Ultrasound Images of the Femoral Cartilage for Guidance in Robotic Knee Arthroscopy.* IEEE Access, 2020. **8**: p. 223961-223975.

44. Ali, S., et al., *Supervised Scene Illumination Control in Stereo Arthroscopes for Robot Assisted Minimally Invasive Surgery.* IEEE Sensors Journal, 2021. **21**(10): p. 11577-11587.

45. Banach, A., et al., *Saliency Improvement in Feature-Poor Surgical Environments Using Local Laplacian of Specified Histograms.* IEEE Access, 2020. **8**: p. 213378-213388.

46. Barreto, J.P., et al. *ArthroNav: Computer assisted navigation system for orthopedic surgery using endoscopic images*. in *1st Portuguese Biomedical Engineering Meeting*. 2011.

47. Jaiprakash, A., et al., *Orthopaedic surgeon attitudes towards current limitations and the potential for robotic and technological innovation in arthroscopic surgery.* J Orthop Surg (Hong Kong), 2017. **25**(1): p. 2309499016684993.

48. Randell, R., et al., *Factors supporting and constraining the implementation of robot-assisted surgery: a realist interview study.* BMJ Open, 2019. **9**(6): p. e028635.

49. Price, A.J., et al., *Evidence-based surgical training in orthopaedics: how many arthroscopies of the knee are needed to achieve consultant level performance?* Bone Joint J, 2015. **97-B**(10): p. 1309-15.

50. Strydom, M., et al., *Robotic Arthroscopy: The Uncertainty in Internal Knee Joint Measurement.* IEEE Access, 2019. **7**: p. 168382-168394.

51. Freisberg, D., et al., *Development of an assistance system for arthroscopic surgery*. 2009, Springer Berlin Heidelberg. p. 186-188.

52. Cooper, D.E., *Single Portal Knee Arthroscopy: 2015 Technique Update.* Arthroscopy Techniques, 2016. **5**(1): p. e17-e22.

53. Ward, B.D. and J.H. Lubowitz, *Basic Knee Arthroscopy Part 1: Patient Positioning.* Arthroscopy Techniques, 2013. **2**(4): p. e497-e499.

54. Mor, A.B. *5 DOF force feedback using the 3 DOF PHANToM and a 2 DOF device*. in *Proceedings of the third PHANToM users group workshop, AI Lab Technical Report*. 1998.

55. EngineeringToolbox. *Polymers - Physical Properties*. 2008; Available from: https://www.engineeringtoolbox.com/polymer-properties-d_1222.html.

56. PolymerDatabase. [cited 2023 March 18]; Available from: https://polymerdatabase.com/polymer%20physics/Poisson%20Table.html.

57. EngineeringToolBox. *Friction - Friction Coefficients and Calculator*. 2004 [cited 2023 March 18]; Available from: https://www.engineeringtoolbox.com/friction-coefficients-d_778.html.

58. Xu, M.-M., et al., *Static and Dynamic Properties of Semi-Crystalline Polyethylene.* Polymers, 2016. **8**(4): p. 77.